Biomaterials Science

ROYAL SOCIETY OF CHEMISTRY

PAPER

View Article Online
View Journal | View Issue

Cite this: *Biomater. Sci.*, 2021, **9**, 2608

Photothermal therapy with silver nanoplates in HeLa cells studied by *in situ* fluorescence microscopy†

María Belén Rivas Aiello,[a] Julio C. Azcárate,[b] Eugenia Zelaya,[b] Pedro David Gara,[c] Gabriela N. Bosio,*[a,d] Thomas Gensch *[d] and Daniel O. Mártire [a]

Photothermal therapy (PTT) is a noninvasive treatment for cancer relying on the incorporation of NIR-light absorbing nanomaterials into cells, which upon illumination release heat causing thermally induced cell death. We prove that irradiation of aqueous suspensions of poly(vinylpyrrolidone)-coated silver nanoplates (PVPAgNP) or PVPAgNP in HeLa cells with red or NIR lasers causes a sizeable photothermal effect, which in cells can be visualized with the temperature sensing fluorophore Rhodamine B (RhB) using spinning disk confocal fluorescence microscopy or fluorescence lifetime imaging. Upon red-light irradiation of cells that were incubated with both, RhB and PVPAgNP at concentrations with no adverse effects on cell viability, a substantial heat release is detected. Initiation of cell death by photothermal effect is observed by positive signals of fluorescent markers for early and late apoptosis. Surprisingly, a new nanomaterial-assisted cell killing mode is operating when PVPAgNP-loaded HeLa cells are excited with moderate powers of fs-pulsed NIR light. Small roundish areas are generated with bright and fast (<1 ns) decaying emission, which expand fast and destroy the whole cell in seconds. This characteristic emission is assigned to efficient optical breakdown initiation around the strongly absorbing PVPAgNP leading to plasma formation that spreads fast through the cell.

Received 16th November 2020,
Accepted 7th February 2021

DOI: 10.1039/d0bm01952f

rsc.li/biomaterials-science

1. Introduction

Photothermal therapy (PTT) is defined as the killing of cancer cells, which have taken up light absorbing particles, that release efficiently heat upon irradiation with NIR (typically laser) light.[1] The development of PTT motivated the attention of researchers to the study of the photo-physical processes causing hyperthermia and leading to cell death.[2]

New prospects for light-activated therapies have recently emerged by exploiting the unique optical properties of noble-metal nanoparticles. When the incoming light couples with the oscillation frequency of the conduction electrons in such nanoparticles, a so called localized surface plasmon resonance (LSPR) arises, which is manifested as a strong absorption band accompanied with an efficient photon-to-heat conversion (photothermal) effect.[3] More specifically, when localized in the tumor, the plasmonic nanoparticles can act as efficient photothermal transducers by converting the light absorbed by surface plasmon resonances into heat, leading to a tightly localized temperature rise determined by the nanoparticle size and the local thermal diffusivity, thereby achieving therapeutic cell killing.[4,5]

Plasmonic nanoparticles based on gold are very popular for PTT applications and have been used as photothermal transducers for the treatment of highly aggressive tumours[6–11] also in combination with immune therapy.[12] In addition, silver-based nanomaterials have also been developed and utilized. For instance, Boca *et al.* conducted cytotoxicity assays and found that chitosan-coated silver nanotriangles exhibited good compatibility for healthy human embryonic cells, while showing a dose-dependent phototoxicity towards NCI-H460 cancer cells upon excitation with 800 nm light.[5] These results motivated us to prepare and characterize polyvinylpyrrolidone (PVP)-coated silver nanoplates (PVPAgNP) to be used in PTT assays with HeLa cells. It has been shown that silver nanoplates and in particular silver nanotriangles are best suited among the different types of silver nanomaterials in PTT appli-

[a]*Instituto de Investigaciones Fisicoquímicas Teóricas y Aplicadas (INIFTA), Facultad de Ciencias Exactas, Universidad Nacional de La Plata, C. C. 16, Suc. 4, (1900) La Plata, Argentina. E-mail: gbosio@inifta.unlp.edu.ar*
[b]*Bariloche Atomic Center, National Atomic Energy Commission – CONICET, Av. Bustillo 9500, 8400 S. C. de Bariloche, Río Negro, Argentina*
[c]*Centro de Investigaciones Ópticas (CIOp), (CONICET La Plata – CIC – UNLP), Cno. Parque Centenario e/505 y 508, Gonnet, Argentina*
[d]*Institute of Complex Systems (IBI-1; Molecular and Cellular Physiology), Forschungszentrum Jülich, Wilhelm-Jonen-Straße, 52428 Jülich, Germany. E-mail: t.gensch@fz-juelich.de*

†Electronic supplementary information (ESI) available. See DOI: 10.1039/d0bm01952f

cations, since their absorption spectra[5,13–16] match well the therapeutic window of biological tissue.[17]

For the purpose of measuring the intracellular PTT effect of our PVPAgNP, we used the fluorescent dye Rhodamine B (RhB) that shows temperature dependent fluorescence quantum yield and fluorescence lifetime change in a relevant temperature range.[18,19]

To prove the ability of the silver nanoplates to act as photothermal agents, herein we report the use of Spinning Disk Confocal Microscopy (SDCM) and Fluorescence Lifetime Imaging Microscopy (FLIM) techniques to monitor changes in the fluorescence intensity and lifetime of the optical thermometer RhB in HeLa cells incubated with RhB and PVPAgNP. We also demonstrate cell killing by illuminating HeLa cells loaded with PVPAgNP by two different photodestruction modes. One uses cw light (here 640 nm) and leads to a local temperature increase with subsequent apoptotic death of the cells. The other method relies on fs-pulsed near infrared light (here 780 nm), where the PVPAg nanoplates act as absorbers and heat emitters for PTT as well as catalysts of a plasma generation that destroyed efficiently and fast (in seconds) the illuminated cells.

2. Materials and methods

2.1. Materials

Silver nitrate was obtained from Biopack (Zárate, Buenos Aires, Argentina) and trisodium citrate from Cicarelli (San Lorenzo, Santa Fe, Argentina), PVP, sodium borohydride ($NaBH_4$), RhB, sodium azide (NaN_3), 3-(4,5-dimethylthiazol-2-yl)-2,5-diphenyltetrazolium bromide (MTT), Neutral Red were purchased from Sigma-Aldrich (St Louis, USA). Hydrogen peroxide was from Anedra (San Fernando, Buenos Aires, Argentina). Annexin V conjugated with fluorescein isothiocyanate (FITC) and propidium iodide (PI) were purchased from BD Biosciences (Heidelberg, Germany). All experiments were performed with deionized water.

2.2. Synthesis of PVP-coated silver nanoplates

As reported previously,[13] 24 mL of pure water, 50 μL of an aqueous solution of silver nitrate (Biopack, 0.05 M), 500 μL trisodium citrate (Na_3cit, J.T. Baker, 75 mM), 100 μL of PVP (Sigma-Aldrich, 17.5 mM), and 60 μL hydrogen peroxide (Anedra, 30 wt%) were mixed and vigorously stirred at room temperature in air. Injection of sodium borohydride ($NaBH_4$, Sigma-Aldrich, 100 mM, 250 μL) was done with automatic pipette immediately after stirring, and after a few seconds the colour of the solution turned from colourless to blue, indicating formation of the PVPAg nanoplates.

2.3. TEM imaging

The characterization of size and shape of the PVPAgNP were performed by FEI Tecnai F20 G2 (FEG) transmission electron microscope operated at 200 kV. Aqueous suspensions of PVPAgNP were drop-casted over copper PELCO® (Ted Pella, Redding, CA, USA) TEM grid with support films of Formvar substrate. The size distribution was determined considering the mean diameter contained into a polyhedron shape (see Fig. S1 in the ESI† for details). The mean size of the formed PVPAg nanoplates was obtained by fitting the size distribution with a LogNormal function. Also, the aspect ratio and shape factor were determined as features of the sample (see Fig. S1 and Table S1 in the ESI†).

2.4. ATR-FTIR microscopy

An Agilent ATR FT-IR 630 spectrophotometer with a spectral range 5100–640 cm^{-1} was employed. The spectral resolution of the equipment is lower than 2 cm^{-1} and its precision is 0.05 cm^{-1}.

2.5. Fluorescence spectroscopy

A HORIBA JOBIN-YVON Spex Fluorolog FL3-11 was employed for measuring fluorescence spectra. Photoluminescence lifetime measurements were performed with the same device with TCSPC technique using excitation with pulsed LED at 575 nm operating at 1 MHz (FWHM ≈1.2 ns).

2.6. Heat production by NIR irradiation

The suspensions of PVPAgNP in pure water (2 mL) contained in 10 mL glass flasks with magnetic stirring were irradiated with either 170 fs laser pulses at a repetition rate of 1 kHz (800 nm, 600 mW) generated by a Ti: sapphire Chirped Pulse Amplification (CPA) system from Spectra Physics (Mai-Tai Spitfire; Newport Spectra Physics, Irvine, CA, USA) or with a continuous wave (cw) He–Ne laser from LaserOptics S.A. (633 nm, 7.2 mW; Buenos Aires, Argentina). The laser beam (spot size: 7 and 6 mm, respectively) was directed to the top of the flasks placed inside a polystyrene container to avoid heat leakage. The temperature was measured using a Lutron PH-206 digital thermometer.

2.7. Incubation of HeLa cells with RhB and PVPAgNP

HeLa cells from the American Type Culture Collection (ATCC CCL-2) were grown in modified Eagle's medium (MEM) (GIBCO – Argentina) containing 10% FBS (Internegocios S.A. – Argentina) and 100 μg mL^{-1} of penicillin. 1.5×10^4 cells were cultured in an incubator with 5% CO_2 and 95% air at 37 °C for 24 h. The medium was then removed, and the cells were incubated with different concentrations of RhB (30 min for imaging experiments or 24 h for cell survival measurements) and/or PVPAgNP (24 h) in MEM. For FLIM experiments, the incorporation of PVPAgNP in the cells was assessed before the incubation with RhB (30 min). Every experiment was compared to a control culture. Cell survival was assessed by MTT and NRU assays as described previously.[20–23]

2.8. Dendra2-Mito expressing HeLa cells

HeLa cells were transfected with DNA encoding a green fluorescent protein decorated with a targeting sequence for the mitochondrial matrix[24] (Dendra2-Mito). Transfection was performed two days before imaging experiments according to a

slightly modified Calcium-phosphate transfection protocol described by Chen and Okayama.[25]

2.9. SDCM

The SDCM instrumentation (Acal BFI, Gröbenzell, Germany and Nikon Instruments Europe BV, Amsterdam, Netherlands) was described previously.[23] PTT-experiments were performed by illuminating HeLa cells that were before incubated with PVPAgNP (or not as control) with red laser light (640 nm: 0.018 W cm^{-2}). For RhB and Dendra2-Mito imaging lasers of 561 nm (0.0016 W cm^{-2}) and 488 nm (0.0013 W cm^{-2}) were used as excitation source, respectively. Cells were kept in a stage-top incubator (Okolab S.R.L., Pozzuoli, Italy) on the microscope during acquisition of microscopy images providing 5% CO_2 atmosphere and temperature control, which was kept at 37 °C if not otherwise stated.

2.10. FLIM in living cells

Fluorescence lifetime images were measured using an upright scanning fluorescence microscope (A1 MP; Nikon Instruments Europe) equipped with a 25× objective (water immersion, numerical aperture 1.1; working distance 2 mm; N25X-APO-MP; Nikon). Fluorescence was excited by 2-photon excitation (<100 fs light pulses; λ_{exc} = 750 nm). Laser pulses were generated using a mode-locked Titan-Sapphire laser (MaiTai DeepSee; output power 2.3 W at 750 nm; Newport Spectra Physics) at a frequency of 80 MHz. Mean fluorescence lifetimes were measured using time-correlated single photon counting (TCSPC). TCSPC electronics and acquisition software (SPC-152; Becker & Hickl) were used for FLIM as previously described.[26,27] SPCImage 4.8 software (Becker & Hickel) was used to fit bi-exponential functions to individual fluorescence decays (bin of 2). The average fluorescence lifetime was determined for each pixel from amplitudes and lifetimes of the two-exponential functions as $(a_1 \times \tau_1 + a_2 \times \tau_2)/(a_1 + a_2)$ (see ref. 28 and discussion therein).

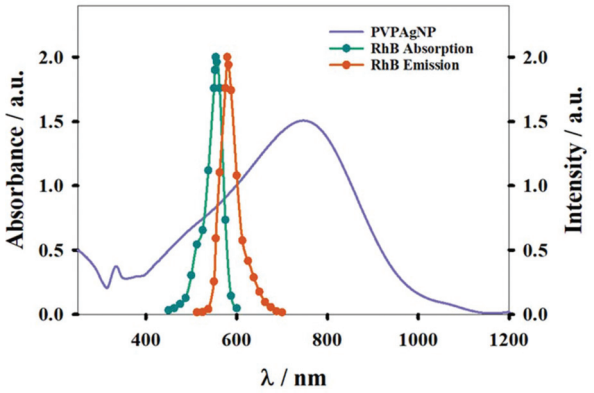

Fig. 1 Absorption spectrum of aqueous suspension of PVPAgNP (left *y*-axis). The normalized absorption and emission spectra of Rhodamine B (right *y*-axis) are also shown.

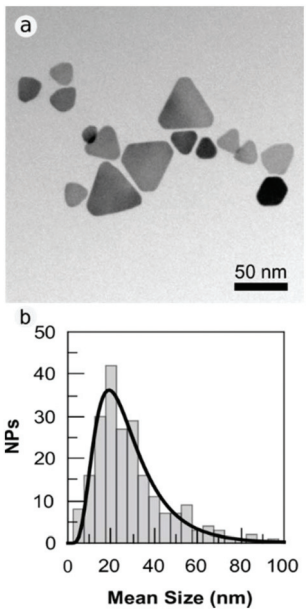

Fig. 2 (a) TEM bright field images of PVPAgNP. The images were acquired slightly over focused to increase the contrast in NP border. (b) Size distribution of the PVPAg nanoplates.

3. Results and discussion

3.1. Characterization of PVPAgNP

Fig. 1 shows absorption spectra of PVPAgNP suspensions (from near UV to near IR) and the excitation and emission fluorescence spectra of RhB. PVPAgNP show high absorbance in the wavelength region of minimal tissue absorbance and autofluorescence, which is located between 650 and 1450 nm.[29] Thus, these nanomaterials is a potential candidate for application in PTT.

Fig. S1 in the ESI† shows how the mean diameter of the PVPAg nanoplates (most of them nanotriangles) was calculated. The mean size of the nanotriangles is 29 ± 16 nm; the aspect ratio is 1.17 and the shape factor is 0.83 (Fig. S1†).

The synthesis protocol of the PVPAg nanoplates gives a nanotriangle yield of approximately 30% with a high polydispersity in size. Also, the rest of the PVPAg nanoparticles shows great polydispersity in size and shape (Fig. 2). This polydispersity is in line with the broad LSPR absorption band characteristic for nanotriangles in the range of 600–900 nm (see Fig. 1). Nevertheless, no significant amount of spherical Ag nanoparticles is observed, which is in agreement with the absence of a LSPR band at around 400 nm.

Notably, the PVPAgNP used here are nanoplates with a high monodispersity in thickness (mean: 2 nm) in agreement with earlier studies on similar nanomaterials.[13,30]

These types of Ag nanoplates are commonly called "lamellar" nanoparticles due the great number of stacking faults in the <111> direction, *i.e.*, parallel to {111} faces of the plates.[30]

The stability of nanomaterials is an important property for biological use and medical application. It was reported that

the triangles could reshape within a few hours after synthesis.[31] However, we found here that the UV-Vis-NIR spectra of aqueous suspensions of the nanoplates stored at room temperature were stable for periods as long as 6 months, indicating their large stability.

The broad, non-structured FTIR band with maximum around 3300 cm^{-1} originates from the O–H vibration of H_2O. The intensity difference between PVP and PVPAgNP reflects the much higher water content of the latter sample (see ESI Fig. S2†). In Fig. S2† a shift of the band of the stretching vibration of the C═O group of PVP to shorter wavenumbers is observed (1660 cm^{-1} for free PVP; 1560 cm^{-1} for PVPAgNP), which is a direct consequence of Ag bonding to PVP. The same behaviour was also observed by Song *et al.* when PVP was bound to Ag nanomaterials of different shape and was assigned to the coordination between Ag^+ and the carbonyl oxygen of PVP.[32] The peak at about 890 cm^{-1} present in the spectrum of PVPAgNP is ascribed to the breathing vibration of the pyrrolidone ring and is reflecting a tilted conformation of the ring on the surface of the silver nanoplates.[33] The peak at ~2950 cm^{-1}, present in both spectra but with higher intensity for PVPAgNP, is assigned to the asymmetric stretching vibrations of CH_2 in the skeletal chain of PVP. The characteristic absorption peaks of C–H groups at 1426 and 1363 cm^{-1} for PVP appear as a broader band with maximum at 1383 cm^{-1} for PVPAgNP. The C–N vibration has a maximum at 1281 cm^{-1} for PVP, which is shifted to 1257 cm^{-1} (PVPAgNP).

3.2. Photothermal effect of PVPAgNP in cuvette

In order to evaluate the photothermal effect of the Ag nanoplates, aqueous suspensions of PVPAgNP (A^{800} = 0.10) were irradiated with a train (80 MHz) of 170 fs pulses of 800 nm laser light. A similar laser was used in the two-photon fluorescence microscopy experiments with HeLa cells (see end of results section). Fig. 3a shows the expected photothermal effect, namely, that prolonged irradiation causes heating of the PVPAgNP suspension, where its temperature increases monotonically and is levelling off at about 30 minutes (irradiation of pure water is shown for comparison). The much lower temperature increase at later times can be explained by the imperfectness of our experimental setup, *i.e.*, heat losses from the heat-isolated cuvette to the surrounding room air. The latter will be more pronounced the higher the temperature of the suspension is in comparison to room temperature. Further cuvette heating experiments were performed with a second irradiation source, similar to the heating laser used in the spinning disk confocal fluorescence microscopy experiments (see below), by irradiation of PVPAgNP suspensions (A^{633} = 0.609) with a cw He–Ne laser, which resulted again in a temperature rise. The latter was independent of the presence RhB, whose absorption is very low at the laser emission wavelength (A^{633} = 0.001). Blank experiments performed with water or RhB solutions without PVPAgNP yielded a much lower temperature rise (Fig. 3b). Since the absorbed energy is much smaller in the case of cw red laser excitation the total temperature increase achieved in one hour is also much lower (*ca.* 10 times) compared to the experiment with excitation at 800 nm (see Fig. 3). Consequently, the levelling off of the temperature increase is not so pronounced and shifted towards later times.

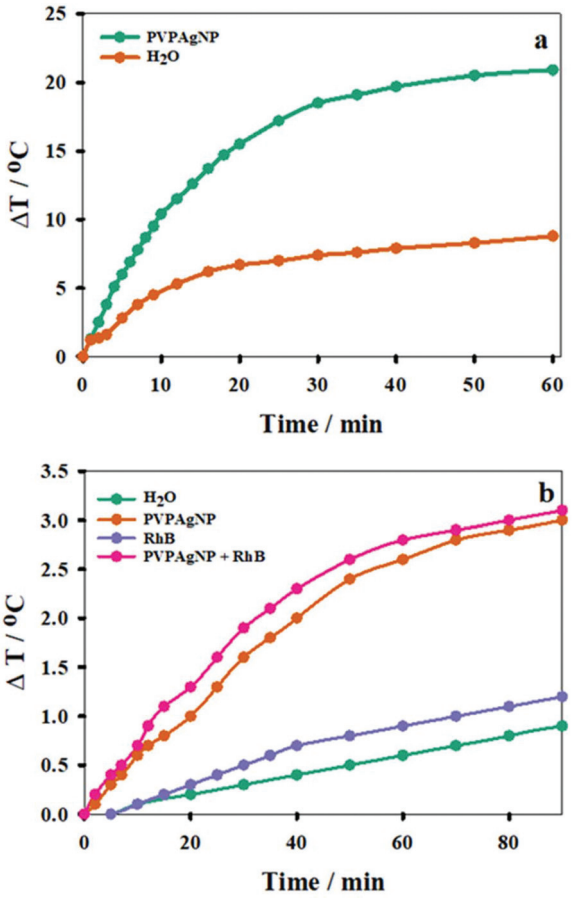

Fig. 3 Temperature increase upon irradiation of: (a) at 800 nm (600 mW Ti: Saphire laser) of a PVPAgNP suspension (A^{800} = 0.10) and water. (b) at 633 nm (7.2 mW He–Ne CW laser) of water; a 2.5 μM RhB solution (A^{633} = 0.001); and a PVPAgNP suspension (A^{633} = 0.609) in the presence or absence of 2.5 μM RhB.

3.3. Viability of cells incubated with PVPAgNP

The concentration of PVPAgNP employed in the biological experiments were chosen with the aid of cell viability experiments. To this purpose, two different tests were employed to check cell viability: the MTT ((3-(4,5-dimethylthiazol-2-yl)-2,5-diphenyltetrazolium bromide) tetrazolium) and the Neutral Red uptake (NRU) assays. The former test is based on the ability of viable cells with active metabolism to convert MTT into formazan, a product with an absorbance maximum at 570 nm.[22,34] The NRU assay evaluates the ability of viable cells to incorporate and keep the NR dye in its protonated form in the lysosomes.[35]

As can be seen in Fig. S3† only the incorporation of RhB at 3.5 μM showed decreased viability. Cell viability was not affected by PVPAgNP for concentrations of up to 10 μM (in Ag) in the culture medium. Thus, all further biological assays were

performed with [RhB] <3.5 μM and PVPAgNP within these concentration ≤10 μM.

3.4. Spinning disk confocal fluorescence microscopy (SDCM)

3.4.1. Cell death caused by photothermal effect in PVPAgNP incubated cells. Annexin V FITC is used along with Propidium iodide (PI) to evaluate if cells are viable, apoptotic, or necrotic through differences in plasma membrane integrity and permeability.[36] Annexin V was shown to be helpful for detection of apoptotic cells because of its binding affinity for the negatively charged phosphatidylserine (PS), exposed to the extracellular surface of the cell at the beginning of apoptotic process.[37] During the early events of apoptosis PS-lipids, which in active cells are actively transported to the inner (cytosolic) leaflet of the plasma membrane by the cell, suffer translocation to the outer (extracellular) leaflet of the plasma membrane.[37–39] PI, a water-soluble dye, whose fluorescence quantum yield increases upon intercalation with DNA while absorption and fluorescence spectra possess considerable red-shifts, only stains late apoptotic and necrotic cells, which have non-intact plasma and nuclear membranes.[40]

Fluorescence images were obtained using a dual window optical beam splitter to measure simultaneously the channels with excitation wavelengths of 488 nm and 561 nm, respectively, employed for the Annexin V FITC and PI tests (see Fig. 4). For these assays HeLa cells were incubated for 24 h with 10 μM of PVPAgNP dissolved in cell medium, then incubated with Annexin V FITC/PI for 15 min and exposed to 11 min irradiation with high (0.018 W cm^{-2}) power of the 640 nm laser of the spinning disk confocal microscope. Already in the bright field images one can clearly see a difference between control (no change of nucleus morphology) and the cell that has taken up PVPAgNP (large change of nucleus morphology). While 60 minutes after the red light irradiation no apoptotic signals were observed in control cells (no membrane staining by Annexin V FITC and no propidium iodide fluorescence from nucleus), cells that have been incubated with PVPAgNP show positive fluorescence signals – already after much shorter time (*e.g.* 35 minutes in the example shown in Fig. 4) – for both apoptosis markers: 1. PS-lipids appear on extracellular surface of plasma membrane indicated by strong plasma staining by Annexin V FITC. 2. Intense fluorescence signal of propidium iodide from nuclear region by intercalating DNA proves non-intact plasma membrane, which allows penetration of membrane impermeable propidium iodide molecules.

These results indicate that incubation of HeLa cells with PVPAgNP suspensions followed by 640 nm irradiation clearly led to photodamage related to both early apoptosis and late apoptosis or necrosis. Note that with a similar excitation wavelength (633 nm), the PVPAgNP were shown to produce a temperature increase (Fig. 3b). In other words, the PVPAg nanoplates taken up by the cell allow cell killing by illumination with red light that is not harmful to cells without PVPAgNP.

3.4.2. Localization of temperature probe rhodamine B. In order to detect the temperature raise by fluorescence spectroscopy we used the temperature-dependent fluorescent dye RhB, whose fluorescence quantum yield, Φ_F, was shown to increase by a factor of 2 between room temperature and 200 K.[18] The corresponding change of its fluorescence lifetime τ_F is consistent with the relation $k_F = \Phi_F/\tau_F$, where k_F is the radiative rate constant.[18,19] A correlated temperature dependence of Φ_F and τ_F has also been observed for RhB dissolved in water in the range of 5 °C to 80 °C.[18,41] The fluorescence of RhB is negligibly pressure sensitive and pH independent above pH 6.[42] In addition, RhB has been used in several microfluidic applications,[42–47] and interestingly, crosses lipid bilayers and biological membranes. In mammalian cells, RhB accumulates in the inner mitochondrial membrane and has been used as a mitochondrial probe.[48] Due to these properties RhB was successfully used as optical thermometer for the measurement of temperature in rat tail tendon samples exposed to radiofrequency electromagnetic fields,[49] to characterize the temperature profile in microfluidic devices[50,51] and

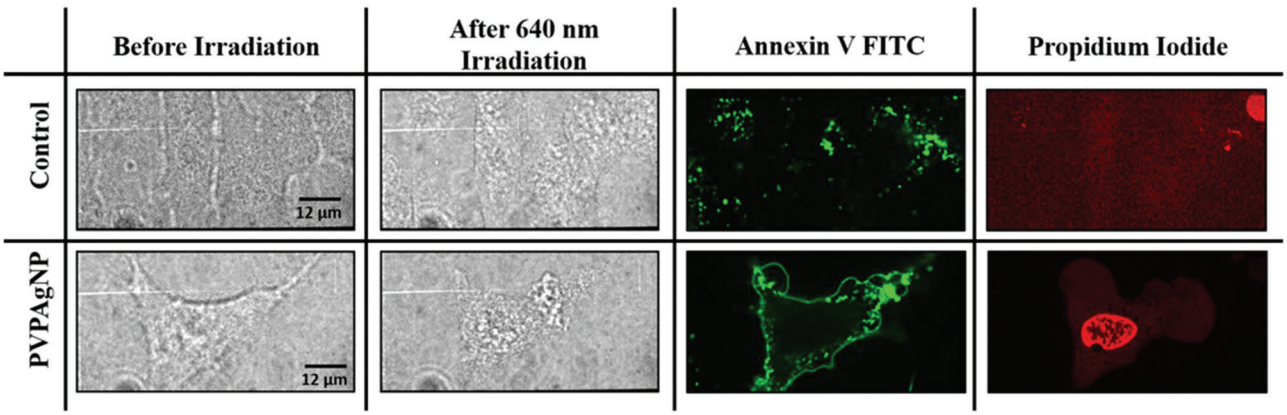

Fig. 4 Summary of the Annexin V/PI tests: On the left, bright-field images of five HeLa cells (control) and one HeLa cell (incubated 24 h with 10 μM PVPAgNP) before and after illumination with 640 nm light (0.018 W cm^{-2}, 11 minutes). On the right, Annexin V FITC (488 nm excitation (0.0013 W cm^{-2}, 0.5 s) and propidium iodide (561 nm excitation (0.0016 W cm^{-2}, 0.5 s)) fluorescence images of the same cells are depicted, where the intensity scales are identical for the experiment with the same excitation wavelength.

in cells exposed to continuous wave microwaves and pulsed lasers.[52,53] We have rechecked the temperature dependence of RhB's fluorescence intensity and lifetime in the absence and presence of PVPAgNP, where we confirmed the behaviour described in the literature and found no influence of PVPAgNP (see Fig. S4 and Table S1†).

Since RhB is used in this study as optical thermometer to prove the photothermal effect of PVPAgNP, we performed an experiment to characterize the highly non-heterogeneous spatial distribution of RhB fluorescence in mammalian cells (Fig. 5–8, S5–S7, and S9†). We compared the spatial distributions of orange-red RhB fluorescence and green Dendra2 fluorescence in HeLa cells transiently transfected with the mitochondria-targeted probe Dendra2-mito, which were incubated with 0.125 μM solution of RhB for 10 min to determine the localization of this dye in HeLa cells. HeLa cells transfected with Dendra2-mito DNA plasmid indeed expressed the fluorescent protein Dendra-2 almost exclusively localized in the mitochondrial matrix. As a result, these cells displayed a strong green signal, specifically localized in mitochondria 6–72 h after transfection. Fluorescence images employing the green (λ_{exc} = 488 nm) and orange-red (λ_{exc} = 561 nm) channels for observation of Dendra2-mito and RhB, respectively (see Fig. S5 in the ESI†), clearly show that RhB localizes largely in mitochondria with a minor fraction in other parts of the cytoplasm, in agreement with literature reports.[54,55]

3.4.3. Rhodamine B fluorescence intensity based temperature measurement in living cells. Once the mainly mitochondrial localization of RhB in HeLa cells was proven, we performed experiments to evaluate the ability of RhB fluorescence to sense temperature changes in HeLa cells. Due to the inhomogeneous spatial distribution, the huge fluorescence intensity differences of RhB in one cell and the large dynamics of the mitochondrial network, as well as the shapes of cell and nucleus, we could not use a simple cell average of the fluorescence intensity. Instead, we tested mean fluorescence intensity values of different selections of pixels as described in Fig. S6† and the corresponding figure caption. $I_{1.5*Inucl}$ was found to be best suited and was used in the following experiments. Fig. 5a shows an experiment, where the same cells have been imaged at 25 °C and subsequently at 37 °C. Direct comparison of left and right image as well as Table 1 undoubtedly demonstrate the decrease of RhB fluorescence intensity in HeLa cells upon heating from 25 °C to 37 °C. The relative change amounted to about −60%.

We also performed the reverse experiment (Fig. 5b and Table 2), namely measuring cells first at 37 °C and afterwards at 25 °C, where we obtained an increase (*ca.* 60%) in RhB fluo-

Table 1 Average fluorescence intensity per cell I_{fl} = $I_{1.5*Inucl}$ (see Fig. S6†) from the five cells observed in Fig. 5a

Cell	$I_{fl,298\ K}$	$I_{fl,310\ K}$	$\Delta I_{fl}/I_{fl,298\ K}$ (%)
I	15 417	5086	−67
II	13 273	5102	−62
III	11 889	4771	−60
IV	8965	4550	−49
V	12 678	5878	−54

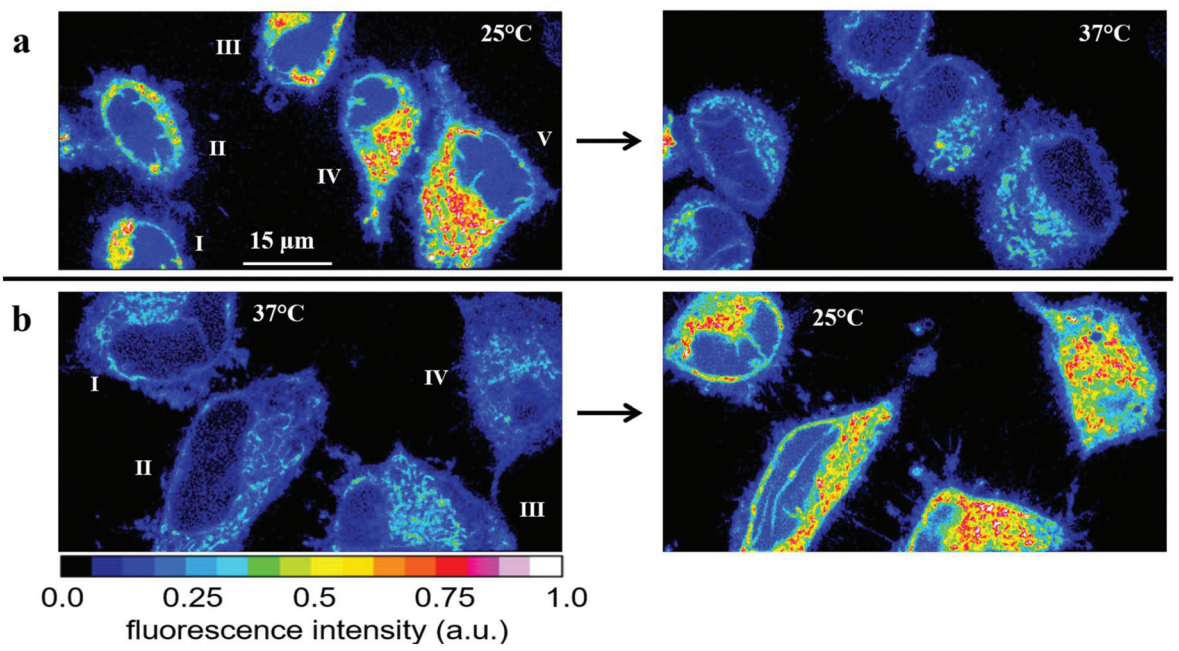

Fig. 5 Temperature effect on the fluorescence intensity of HeLa cells incubated for 30 min with 2.5 μM RhB. (a) Fluorescence images of five cells obtained first at 25 °C (left) and subsequently at 37 °C (right). The average fluorescence intensities I_{fl} = $I_{1.5*Inucl}$ (see Fig. S6†) and the relative changes are depicted in Table 1. (b) Fluorescence images of another set of four cells obtained first at 37 °C (left) and subsequently at 25 °C (right). The average fluorescence intensities I_{fl} = $I_{1.5*Inucl}$ (see Fig. S6†) and the relative changes are depicted in Table 2.

Table 2 Average fluorescence intensity per cell I_{fl} = $I_{1.5*Inucl}$ (see Fig. S6†) from the five cells observed in Fig. 5b

Cell	$I_{fl,310\ K}$	$I_{fl,298\ K}$	$\Delta I_{fl}/I_{fl,298\ K}$ (%)
I	4109	10 166	60
II	3746	10 533	64
III	5020	13 015	61
IV	4085	11 363	64

Table 3 Fluorescence intensity per cell I_{fl} = $I_{1.5*Inucl}$ (see Fig. S6†) and relative change of the two cells observed in Fig. 6 upon 640 nm light irradiation

Cell	$I_{fl,\ before\ 640\ nm}$	$I_{fl,\ 640\ nm\ (1\ min)}$	$I_{fl,\ 640\ nm\ (6\ min)}$
I	12 075	11 377 (−5.8%)	9315 (−23%)
II	11 387	10 908 (−4.2%)	9214 (−19%)

rescence of very similar size (*ca.* 60%) compared to the decrease determined in the experiment depicted in Fig. 5a. This proves the suitability of the method and the absence of significant RhB photobleaching under the experimental conditions applied here. Photobleaching would lead to an apparent temperature increase, which was excluded by the latter experiment. Thus, the fluorescence intensity of RhB can be used as an optical thermometer in HeLa cells for detecting relative temperature changes. Since fluorescence intensity is proportional to number of dye molecules and passive loading of cells with RhB cannot be precisely controlled we did not try to calibrate the fluorescence change as a function of temperature. Therefore, absolute temperatures cannot be measured in our experimental setup.

3.4.4. Heat release by irradiation of PVPAgNP visualized by RhB fluorescence in living cells. Once we had established RhB fluorescence intensity of cells as a relative measure of temperature we designed an experiment to visualize the basis of the photothermal effect, namely a heat release upon absorption of light by the PVPAgNP. For this purpose, HeLa cells were incubated with PVPAgNP (24 h) and RhB (30 min). The cells were held at 25 °C (to reduce mobility of cells and mitochondria) and irradiated with strong light of a 640 nm laser. Fig. 6 shows such an experiment, where both cells show already after 1 min a decrease of RhB fluorescence intensity (of a few percent; see Fig. 6b, c and Table 3). This behaviour is augmented after an additional five minutes 640 nm irradiation period, where the RhB fluorescence intensity is now decreased by about 20% (see Fig. 6d and Table 3). In light of the results of the previous section, this fluorescence decrease has to be interpreted as a large-scale heat release and temperature increase. The irradiation light for heating was chosen in such a way, that it is efficiently absorbed by the PVPAgNP, but not absorbed by RhB nor the vast majority of naturally occurring absorbing molecules of the cell to prevent photobleaching (of RhB) and photodamage (of the cells). In fact, a control experiment that was identically designed to the one shown in Fig. 6 with one exception – no incubation with and therefore absence of PVPAgNP – showed only small RhB fluorescence intensity changes of the cells with no explicit trend (Fig. S7 and Table S3†). Therefore, the decrease of RhB fluorescence intensity is a direct proof of a large heat release in PVPAgNP-containing HeLa cells, which in turn is very likely the cause of the cell-killing, *i.e.*, the photothermal effect of PVPAgNP irradiation (see Fig. 4), though other phototoxic effects cannot be ruled out. In addition, it demonstrates the possibility of detection of heat releases in cells employing RhB as an optical thermometer.

3.5. Fluorescence lifetime imaging (FLIM) and cell killing by plasma generation

Acquisition of fluorescence intensity and fluorescence lifetime images of HeLa cells incubated with RhB alone or RhB and PVPAgNP was performed according to the following protocol:

1. Images of an area with several cells were acquired with the excitation laser set at 880 nm (10 mW).

2. Images of one or two cells were obtained from a smaller part of the first image with the excitation laser set at 780 nm (12 mW).

3. Step 1 was repeated to compare fluorescence intensity and lifetime images of cells either irradiated with 780 nm light or not.

The irradiation time in each step was 80 s.

Fig. 7 shows the fluorescence intensity and lifetime images obtained from HeLa cells incubated with RhB and PVPAgNP,

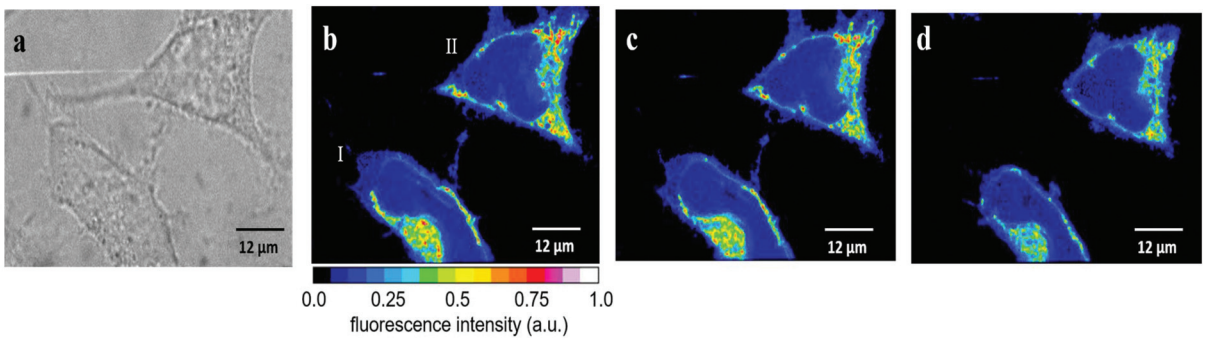

Fig. 6 640 nm irradiation effect on the fluorescence intensity of HeLa cells incubated with 10 µM PVPAgNP (24 h) and 2.5 µM RhB (30 min) at 25 °C. (a) Bright field image and fluorescence images obtained before (b), after 1 min (c), and after 6 min (d) irradiation with 640 nm light.

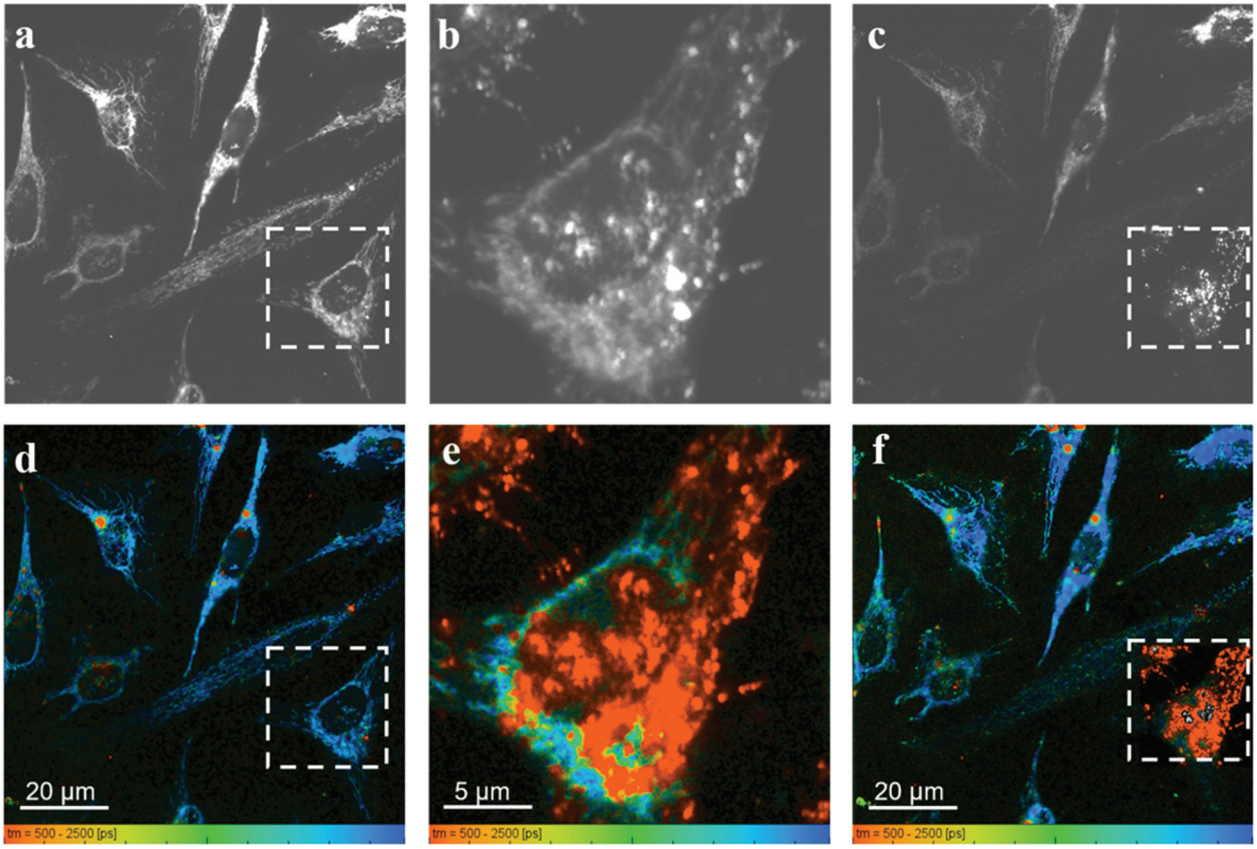

Fig. 7 Fluorescence intensity and lifetime images of HeLa cells incubated 24 h with 10 μM PVPAgNP (6 h) and RhB (30 min) was obtained with 880 nm excitation (10 mW) excitation (a and d). Afterwards the square marked with a dashed white line was illuminated with 780 nm light (12 mW) (b and e). At last the larger area was excited again with low power 880 nm (10 mW) excitation (c and f).

according to the previous protocol. It can be clearly seen that 780 nm irradiation of HeLa cells previously incubated with PVPAgNP generates roundish, spot-like areas with high fluorescence intensity and short, multi-exponential fluorescence decays visible both with 780 nm (Fig. 7b and e) as well as 880 nm excitation (Fig. 7c and f). Notably, the spatial fluorescence intensity distribution and the fluorescence lifetimes are unchanged in the cells not illuminated with 780 nm (compare Fig. 7a and d with Fig. 7c and f). These newly emerging fluorescent islands appear first after a few seconds when acquiring Fig. 7b and e, while their number and strength grows fiercely during the 80 seconds scan with 780 nm light. To explain this behaviour, we need to examine in more detail what the fs-pulsed near-infrared light (780 and 880 nm) is causing in the cells loaded with PVPAg nanoplates and RhB. First, RhB has a large two-photon absorption cross section[56,57] and will be excited by two-photon absorption and generate RhB fluorescence mainly in the mitochondria, where RhB is preferentially located. Its fluorescence decay is found to be mono-exponential with a lifetime between 2.2 and 2.4 ns (Fig. S8a†) and it is the dominant signal in Fig. 7d and f except for the cells that were illuminated by 780 nm light. Second, PVPAgNP will absorb near-infrared light efficiently according to their absorption spectrum (Fig. 1) and release heat. Since 780 nm is very near to the absorption maximum of PVPAgNP, while at 880 nm the absorption is three times lower, this local heat dissipation around the (non-fluorescent) PVPAgNP will be much more pronounced in the second experiment with 780 nm excitation (Fig. 7b and e). Third, various endogenous fluorophores get excited *via* two-photon absorption at both wavelengths leading to so-called autofluorescence distributed over the whole visible spectrum.[58–60] Naturally, autofluorescence has highly multiexponential fluorescence decays and is dominated by contributions of NaDH/NAD^+ as well as protein-bound or free FAD with average fluorescence lifetimes between 1 and 2 ns (photobleached areas in Fig. 7c, f and S8b†) for the two-photon excitation range used here.[61] The last process is a third contribution to the fluorescence characterized by roundish very bright fluorescent spots, which appear both in cytoplasm as well as in the nucleus while irradiating the PVPAgNP loaded cells with 780 nm light. These newly formed fluorescent centres are not only very bright but show also a characteristic very short though non-monoexponential decay (Fig. 7b, e, 8c, f and S8c†). It has to be noted that the RhB fluorescence decay near to such fluorescent centres has a more light-blue and green colour indicating shorter lifetimes of 1.5–2.1 ns, when excited with 780 nm, the wavelength of maximal absorption, *i.e.*, maximal heat release around the PVPAgNP. Since

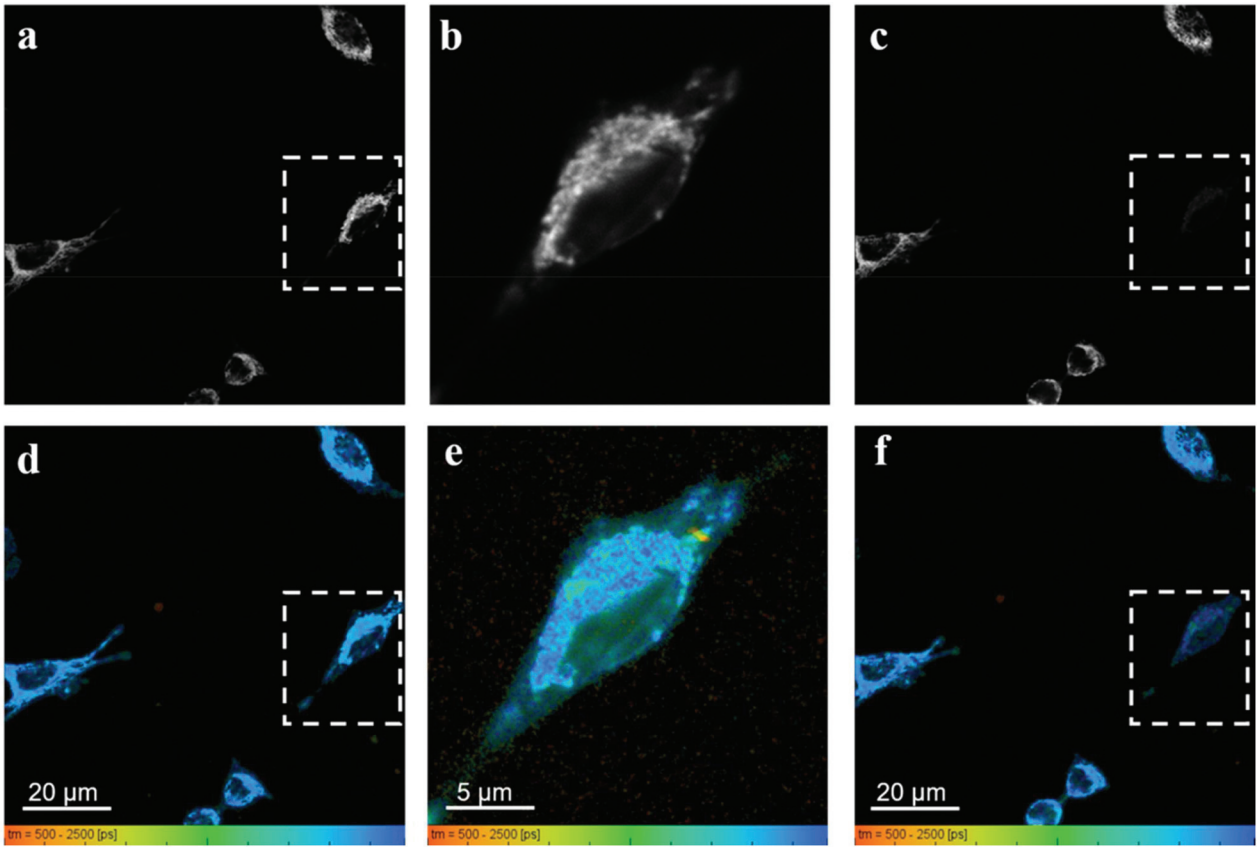

Fig. 8 Fluorescence intensity and lifetime images of HeLa cells incubated with RhB (30 min) but not with PVPAgNP was obtained with 880 nm excitation (10 mW) excitation (a and d). Afterwards the square marked with a dashed white line was illuminated with 780 nm light (12 mW) (b and e). At last the larger area was excited again with low power 880 nm (10 mW) excitation (c and f).

RhB fluorescence lifetime is indeed getting shorter with increasing temperature[18,41,62] (Table 1), the observed shorter fluorescence decays could be interpreted as local heating.

In control experiments, where HeLa cells were stained with RhB but not incubated with and therefore not containing PVPAgNP (Fig. 8), excitation with strong 780 nm light (Fig. 8b and e) leads only to pronounced photobleaching of RhB fluorescence intensity but no fluorescence lifetime change (Fig. 8c and f). Two hallmark observation of the previous experiment, the intense roundish spots of intense fluorescence with very short fluorescence decay as well as the apparent shortening of the RhB fluorescence lifetime, are absent. Consequently, we assign these two phenomena to the efficient absorption of 780 nm light by the PVPAg nanoplates, where the enhanced photothermal effect is causing the observed fluorescence and morphological changes leading to cell destruction.

We have demonstrated that there is a photothermal effect upon NIR excitation of both, suspensions of PVPAgNP and HeLa cells incubated with PVPAgNP (see above), but the generation of the short lived emission observed in the FLIM experiments could be a physiological response of the cell upon generation of singlet molecular oxygen, $O_2(^1\Delta_g)$, photosensitized by PVPAgNP. For silver nanomaterials it was proposed that only nanostructures having the Ag(111) surface, such as Ag decahedrons and Ag triangular plates as those employed in the present study, can photosensitize the production of $O_2(^1\Delta_g)$.[63] Thus, FLIM experiments were performed with cells incubated with NaN_3, a well-known $O_2(^1\Delta_g)$ quencher.[64] Fig. S9 (ESI†) shows that irradiation of HeLa cells incubated with RhB, PVPAgNP and NaN_3, does not preclude the generation of the short lifetime areas upon irradiation at 780 nm. Unfortunately, our experiments are not designed as such that we could evaluate whether bright emissive spots with very short fluorescence decays are formed to a lesser or the same extent in the presence or absence of NaN_3. But we can conclude that the effect of NaN_3 is not sufficiently protective, thus further supporting the involvement of the photothermal mechanism responsible for the photodamage as we have proven here for continuous excitation (640 nm) and one-photon absorption (see above, Fig. 4 and 6).

The very different nature and extent of photodestruction of cells loaded with PVPAgNP for the two excitation modes (cw 640 nm laser or fs-pulsed 780 nm laser) let us search for other possible mechanisms. An obvious hypothesis to explain the observation of areas with bright fluorescence and very short fluorescence decays (as exemplary shown in Fig. S8c, 7f and Fig. S9d, h† is a photosensitized or photochemically induced biochemical process in cells previously incubated with

PVPAgNP and subjected to NIR (780 nm) light, where the absorption of the light by the PVPAg NPs results in the generation of free NADH. NADH is one of the most prominent contributors to cellular autofluorescence and it is long known that the fluorescence decay of unbound NADH is very short. Chance and Thorel showed that NADH exhibits autofluorescence, whereas the oxidized form NAD^+ is not fluorescent.[65,66] This allows microscopic determination of the NAD(H) redox state by measuring NADH fluorescence intensity and lifetime.[67,68] Several research groups reported fluorescence lifetime values for unbound NADH (400 ps; free in solution) and NADH bound to proteins, where the mean fluorescence lifetime varies between 1.0 and 4.0 ns, dependent on its microenvironment.[67,69–71] The ratio of free to protein-bound NADH correlates with the NAD(H) redox state, which can be evaluated from measurements of the mean NADH lifetime, and allows analysis of the metabolic state of cells. There are numerous studies using this so-called metabolic imaging (of autofluorescence upon excitation with near-infrared fs-pulsed lasers,[72] but in none of them a fluorescence lifetime component shorter than 400 ps is reported.[73–75] The nature of the very fast, multiexponential fluorescence decay associated with the here observed bright fluorescent spots caused by illumination of cells, which were incubated with PVPAgNP (Fig. 7b, c, d, e, f and Fig. S9b†), however, does not fit to these studies[73–75] where an enhanced free NADH concentration was observed. The major fluorescence decay component (relative amplitude >95%) that we find in the bright spots has a fluorescence lifetime of 50–80 ps, *i.e.* about five to eight times shorter compared to the fluorescence lifetime of free NADH. We therefore conclude that the generation of free NADH cannot be the cause of the emerging ultrafast fluorescence emission.

If one carefully studies the literature on establishing two-photon fluorescence microscopy with fs lasers in the early 1990s one finds several reports on an emission that was generated while imaging with apparently obviously too high excitation powers. An extensive description of this phenomenon has been given by König *et al.* with the somewhat surprising conclusion that optical breakdown events are generating an electron plasma inside the cell which is emitting light in the whole visible spectrum. The signature of its fluorescence decays is very similar to the one we found in the 780 nm photogenerated bright fluorescent spots with a dominating fluorescence lifetime component faster than 100 ps.[76–78] The plasma formation in an optical breakdown event is essentially the efficient formation of quasi-free electrons involving photoionization and avalanche ionization causing very high photon densities, which are easily achieved in modern fs-pulsed lasers.[79] Optical breakdown and therefore plasma formation can occur without optical absorption but are strongly enhanced when the material is absorbing. König and co-workers investigated the bright luminescence emitted in optical breakdown events during two-photon excitation fluorescence microscopy in great detail and report a number of astonishing details. The luminescence is distributed over the whole visible spectrum. The shorter the pulse width and the wavelength the more intense luminescence is formed. They also observed that the start of optical breakdown usually was in the perinuclear region with a high density of mitochondria, which they suggested to be initiation sites for the optical breakdown. Once some plasma has been formed and is distributing throughout the cell it is formed everywhere when excited again. These descriptive properties are strikingly similar to our observations and we therefore assign our bright luminescent spots to optical breakdown. The control experiment shown in Fig. 8 delivers very important information, namely, that the optical breakdown under our illumination conditions only takes place in the presence of PVPAgNP. They absorb strongly at 780 nm (and much less at 880 nm, where no optical breakdown events occur) and hence we conclude that they enhance the probability of optical breakdown significantly by an unknown mechanism but very likely involving (multiple) absorption events. Interestingly, the only difference to the observations by König and co-workers is, that in our case initiation centres of optical breakdown are both in the perinuclear region near mitochondria but also inside the nucleus (see Fig. 7b and e). This could be explained by PVPAg nanoplates that enter the nucleus and enhance the optical breakdown also there. To summarize, we found here a new way for photodestruction of cells using moderate powers of fs-pulsed near infrared light and Ag nanomaterials (here PVPAgNP) as inducers for optical breakdown, plasma formation and efficient immediate destruction of mammalian cells. With cell-specific targeted import of such Ag nanoplates in cells of interest (tumors) and fs-pulsed laser excitation between 700 and 800 nm clinically relevant methods can be developed since it will work also through endoscopes.

4. Conclusions

In vitro tests show that NIR irradiation of the photostable and well-dispersed suspensions of PVPAg nanoplates leads to a significant temperature increase. Thus, our nanoplates seem to fulfil the requirements of a photothermal agent to be employed in PTT. Therefore, we irradiated HeLa cells previously incubated with suspensions of PVPAgNP and performed a series of SDCM and FLIM microscopy measurements, which led us to the following conclusions:

(i) The dye RhB can be employed as an optical indicator of the temperature increase following NIR irradiation of HeLa cells.

(ii) Annexin V and PI show that one-photon photoexcitation with continuous light (640 nm) of cells incubated with PVPAgNP leads to cell death by both necrosis and/or apoptosis.

(iii) Irradiation of HeLa cells preincubated with PVPAgNP with fs-pulsed laser light (780 nm) results in the generation of areas with bright luminescence with very short fluorescence decays. Cells, where such bright spots were formed, changed their morphology drastically within a minute and were

destroyed almost immediately. We attribute this to efficient optical breakdown initiation around the strongly absorbing PVPAg nanoplates leading to plasma formation that spreads through the whole cell.

Author contributions

M. B. R. A. synthesized the PVPAgNPs, performed experiments and analysed data; J. C. A., and E. Z. performed TEM imaging of PVPAgNPs; P. M. D. G. and M. B. R. A. carried out the cuvette photothermal heating experiments; G. N. B., D. O. M. and T. G. performed fluorescence microscopy experiments; G. N. B. and T. G. analysed fluorescence microscopy data; M. B. R. A., G. N. B., D. O. M. and T. G. wrote the original manuscript; all authors contributed to the final manuscript; G. N. B., D. O. M. and T. G. supervised the project.

Conflicts of interest

There are no conflicts to declare.

Acknowledgements

This work has been supported by grants PICT 2016-0974 and PICT 2017-1628 from ANPCyT, Argentina. G. N. B.'s work in the laboratory of T. G. was financed by a grant from the Federal Ministry of Education and Research (OptoSys, FKZ 031A16) of the Federal Republic of Germany. M. B. R. A. thanks CONICET for a graduate studentship. G. N. B., J. C. A. and E. Z. are permanent research staff of CONICET, Argentina. P. M. D. G. and D. O. M. are permanent research staff of CIC, Buenos Aires, Argentina.

References

1 V. Shanmugam, S. Selvakumar and C. S. Yeh, *Chem. Soc. Rev.*, 2014, **43**(17), 6254.
2 L. Jauffred, A. Samadi, H. Klingberg, P. M. Bendix and L. B. Oddershede, *Chem. Rev.*, 2019, **119**(13), 8087.
3 E. S. Day, J. G. Morton and J. L. West, *J. Biomech. Eng.*, 2009, **131**(7), 074001.
4 V. P. Zharov, V. Galitovsky and M. Viegas, *Appl. Phys. Lett.*, 2003, **83**(24), 4897–4899.
5 S. C. Boca, M. Potara, A. M. Gabudean, A. Juhem, P. L. Baldeck and S. Astilean, *Cancer Lett.*, 2011, **311**(2), 131–140.
6 H. Huang and M. El-Sayed, *Alexandria J. Med.*, 2011, **47**, 1–9.
7 S. Lal, S. E. Clare and N. J. Halas, *Acc. Chem. Res.*, 2008, 1842–1851.
8 J. R. Cole, N. A. Mirin, M. W. Knight, G. P. Goodrich and N. J. Halas, *J. Phys. Chem. B*, 2009, **113**, 12090–12094.
9 C. Ayala-Orozco, C. Urban, M. W. Knight, A. S. Urban, O. Neumann, S. W. Bishnoi, S. Mukherjee, A. M. Goodman, H. Charron, T. Mitchell, M. Shea, R. Roy, S. Nanda, R. Schiff, N. J. Halas and A. Josh, *ACS Nano*, 2014, **8**, 6372–6381.
10 N. Fernandes, A. C. F. Rodrigues, A. F. Moreira and L. Correia, *Biomater. Sci.*, 2020, **8**, 2990–3020.
11 M. S. Kang, S. Y. Lee, K. S. Kim and D.-W. Han, *Pharmaceutics*, 2020, **12**, 701.
12 T. Shang, X. Yu, S. Han and B. Yang, *Biomater. Sci.*, 2020, **8**, 5241–5259.
13 Q. Zhang, N. Li, J. Goebl, Z. Lu and Y. Yin, *J. Am. Chem. Soc.*, 2011, **133**, 18931–18939.
14 Y. Sun, B. Mayers and Y. Xia, *Nano Lett.*, 2003, **3**, 675–679.
15 B. J. Wiley, S. H. Im, Z.-Y. Li, J. McLellan, A. Siekkinen and Y. Xia, *J. Phys. Chem. B*, 2006, **110**, 15666–15675.
16 C. M. Cobley, S. E. Skrabalak, D. J. Campbell and Y. Xia, *Plasmonics*, 2009, **4**, 171–179.
17 R. Weissleder, *Nat. Biotechnol.*, 2011, **19**, 316–317.
18 T. Karstens and K. Kobs, *J. Phys. Chem.*, 1980, **84**, 1871–1872.
19 R. F. Kubin and A. N. Fletcher, *J. Lumin.*, 1982, **27**(4), 455–462.
20 P. R. Twentyman and M. Luscombe, *J. Cancer*, 1987, **56**(3), 279–285.
21 T. Mosmann, *J. Immunol. Methods*, 1983, **65**, 55–63.
22 J. C. Stockert, R. W. Horobin, L. L. Colombo and A. Blázquez-Castro, *Acta Histochem.*, 2018, **120**(3), 159–167.
23 M. B. Rivas Aiello, D. Castrogiovanni, J. Parisi, J. C. Azcárate, F. S. García Einschlag, T. Gensch, G. N. Bosio and D. O. Mártire, *Photochem. Photobiol.*, 2018, **19**, 1–8.
24 Y. Tang, L. Dai, X. Zhang, J. Li, J. Hendriks, X. Fan, N. Gruteser, A. Meisenberg, A. Baumann, A. Katranidis and T. Gensch, *Sci. Rep.*, 2015, **5**, 11073.
25 C. Chen and H. Okayama, *Mol. Cell. Biol.*, 1987, **7**(8), 2745–2752.
26 T. Gensch, V. Untiet, A. Franzen, P. Kovermann and C. Fahlke, *Photodynamic Therapy in HeLa Cells Incubated with Riboflavin and Pectin-coated Silver Nanoparticles*, Springer International Publishing, Cham, 2015, vol. 111, pp. 189–211.
27 V. Untiet, P. Kovermann, N. J. Gerkau, T. Gensch, C. R. Rose and C. Fahlke, *Glia*, 2017, **65**(2), 388–400.
28 A. Sillen and Y. Engelborghs, *Photochem. Photobiol.*, 1998, **67**, 475–486.
29 R. Wang and F. Zhang, *J. Mater. Chem. B*, 2014, **2**(17), 2422–2443.
30 D. Aherne, D. M. Ledwith, M. Gara and J. M. Kelly, *Adv. Funct. Mater.*, 2008, **18**(14), 2005–2016.
31 M. J. Banholzer, N. Harris, J. E. Millstone, G. C. Schatz and C. A. Mirkin, *J. Phys. Chem. C*, 2010, **114**(16), 7521–7526.
32 Y. J. Song, M. Wang, X. Y. Zhang, J. Y. Wu and T. Zhang, *Nanoscale Res. Lett.*, 2014, **9**(1), 1–8.
33 Y. Gao, P. Jiang, D. F. Liu, H. J. Yuan, X. Q. Yan, Z. P. Zhou, J. X. Wang, L. Song, L. F. Liu, W. Y. Zhou, G. Wang, C. Y. Wang, S. S. Xie, J. M. Zhang and D. Y. Shen, *J. Phys. Chem. B*, 2004, **108**(34), 12877–12881.
34 W. Li, J. Zhou and Y. Xu, *Biomed. Rep.*, 2015, **3**(5), 617–620.
35 G. Repetto, A. del Peso and J. L. Zurita, *Nat. Protoc.*, 2008, **3**(7), 1125–1131.

36 I. Vermes, C. Haanen, H. Steffens-Nakken and C. A. Reutellingsperger, *J. Immunol. Methods*, 1995, **184**(95), 39–51.
37 P. F. R. Palma, G. L. Baggio, C. Spada, R. D. Silva, S. I. Ferreira and A. Treitinger, *J. Infect. Dis.*, 2008, **12**, 108–114.
38 H. M. Hankins, R. D. Baldridge, P. Xu and T. R. Graham, *Traffic*, 2015, **16**(1), 35–47.
39 R. Hingorani, J. Deng, J. Elia, C. McIntyre and D. Mittar, Detection of apoptosis using the BD annexin V FITC assay on the BD FACSVerse™ system, *BD Biosciences*, San Jose, 2011, pp. 1–12.
40 A. M. Rieger, K. L. Nelson, J. D. Konowalchuk and D. R. Barreda, *J. Visualized Exp.*, 2011, **50**, 3–6.
41 C. Paviolo, A. H. A. Clayton, S. L. Mcarthur and P. R. Stoddart, *J. Microsc.*, 2013, **250**(3), 179–188.
42 J. J. Shah, S. G. Sundaresan, J. Geist, D. R. Reyes, J. C. Booth, M. V. Rao and M. Gaitan, *J. Micromech. Microeng.*, 2007, **17**(11), 2224–2230.
43 U. Seger-Sauli, M. Panayiotou, S. Schnydrig, M. Jordan and P. Renaud, *Electrophoresis*, 2005, **26**(11), 2239–2246.
44 L. Gui and C. L. Ren, *Appl. Phys. Lett.*, 2008, **92**(2), 024102.
45 D. Ross, M. Gaitan and L. E. Locascio, *Anal. Chem.*, 2001, **73**(17), 4117–4123.
46 P. Löw, B. Kim, N. Takama and C. Bergaud, *Small*, 2008, **4**(7), 908–914.
47 J. Sakakibara and R. J. Adrian, *Exp. Fluids*, 2004, **37**(3), 331–340.
48 P. Reungpatthanaphong, S. Dechsupa, J. Meesungnoen, C. Loetchutinat and S. Mankhetkorn, *J. Biochem. Biophys. Methods*, 2003, **57**(1), 1–16.
49 Y. Y. Chen and A. W. Wood, *Bioelectromagnetics*, 2009, **30**(7), 583–590.
50 R. K. P. Benninger, Y. Koç, O. Hofmann, J. Requejo-Isidro, M. A. A. Neil, P. M. W. French and A. J. DeMello, *Anal. Chem.*, 2006, **78**, 2272–2278.
51 M. A. Bennet, P. R. Richardson, J. Arlt, A. McCarthy, G. S. Buller and A. C. Jones, *Lab Chip*, 2011, **11**, 3821–3828.
52 S. Kohler, R. P. O'Connor, T. D. T. Vu, P. Leveque and D. Arnaud-Cormos, *IEEE Trans. Microwave Theory Tech.*, 2013, **61**(5), 2015–2022.
53 D. Moreau, C. Lefort, R. Burke, P. Leveque and R. P. O'Connor, *Biomed. Opt. Express*, 2015, **6**(10), 4105–4117.
54 L. V. Johnson, M. L. Walsh and L. B. Chen, *Proc. Natl. Acad. Sci. U. S. A.*, 1980, **77**(2), 990–994.
55 P. Reungpatthanaphong, S. Dechsupa, J. Meesungnoen, C. Loetchutinat and S. Mankhetkorn, *J. Biochem. Biophys. Methods*, 2003, **57**, 1–16.
56 C. Xu, W. Zipfel, J. B. Shear, R. M. Williams and W. W. Webb, *Proc. Natl. Acad. Sci. U. S. A.*, 1996, **93**(20), 10763–10768.
57 N. S. Makarov, M. Drobizhev and A. Rebane, *Opt. Express*, 2008, **16**(6), 4029–4047.
58 G. A. Wagnières, W. M. Star and B. C. Wilson, *Photochem. Photobiol.*, 1998, **68**(5), 603–632.
59 M. Y. Berezin and S. Achilefu, *Chem. Rev.*, 2010, **110**(5), 2641–2684.
60 A. C. Croce and G. Bottiroli, *Eur. J. Histochem.*, 2014, **58**(4), 320–337.
61 C. Stringari, L. Abdeladim, G. Malkinson, P. Mahou, X. Solinas, I. Lamarre, S. Brizion, J. B. Galey, W. Supatto, R. Legouis, A. M. Pena and E. Beaurepaire, *Sci. Rep.*, 2017, **7**(1), 1–11.
62 R. Mercadé-Prieto, L. Rodriguez-Rivera and X. D. Chen, *Photochem. Photobiol. Sci.*, 2017, **16**(11), 1727–1734.
63 R. Vankayala, A. Sagadevan, P. Vijayaraghavan, C. L. Kuo and K. C. Hwang, *Angew. Chem., Int. Ed.*, 2011, **50**(45), 10640–10644.
64 M. A. Rubio, D. A. Mártire, S. E. Braslavsky and E. A. Lissi, *J. Photochem. Photobiol., A*, 1992, **66**(2), 153–157.
65 B. Chance, *Science*, 1954, **120**(3124), 767–775.
66 B. Chance and B. Thorell, *Nature*, 1959, **184**(4691), 931–934.
67 R. Datta, T. M. Heaster, J. T. Sharick, A. A. Gillette and M. C. Skala, *J. Biomed. Opt.*, 2020, **25**(7), 071203.
68 P. M. Schaefer, S. Kalinina, A. Rueck, C. A. F. von Arnim and B. von Einem, *Cytometry, Part A*, 2019, **95**(1), 34–46.
69 T. G. Scott, R. D. Spencer, N. J. Leonard and G. Weber, *J. Am. Chem. Soc.*, 1970, **92**(3), 687–695.
70 H. Schneckenburger, *Opt. Eng.*, 1992, **31**(7), 1447.
71 J. R. Lakowicz, H. Szmacinski, K. Nowaczyk and M. L. Johnson, *Proc. Natl. Acad. Sci. U. S. A.*, 1992, **89**(4), 1271–1275.
72 O. I. Kolenc and K. P. Quinn, *Antioxid. Redox Signaling*, 2019, **30**, 875–889.
73 D. K. Bird, L. Yan, K. M. Vrotsos, K. W. Eliceiri, E. M. Vaughan, P. J. Keely, J. G. White and N. Ramanujam, *Cancer Res.*, 2005, **65**(19), 8766–8773.
74 K. Awasthi, D. Moriya, T. Nakabayashi, L. Li and N. Ohta, *J. Photochem. Photobiol., B*, 2016, **165**, 256–265.
75 X. Liang, H. Wang, X. Liu and M. Roberts, Proc. SPIE 10013 SPIE BioPhotonics Australasia, 2016, (100131), 4pp.
76 K. König, P. T. C. So, W. W. Mantulin, B. J. Tromberg and E. Gratton, *J. Microsc.*, 1996, **183**, 197–204.
77 K. König, *J. Microsc.*, 2000, **200**(2), 83–104.
78 K. König, *Handb. Biol. Confocal Microsc*, 3rd edn, 2006, pp. 680–689.
79 A. Vogel, J. Noack, G. Hüttman and G. Paltauf, *Appl. Phys. B: Lasers Opt.*, 2005, **81**(8), 1015–1047.